

Kernel canonical correlation analysis approximates operators for the detection of coherent structures in dynamical data

Stefan Klus,^{1, a)} Brooke E. Husic,^{1, 2, b)} and Mattes Mollenhauer^{1, c)}

¹⁾Department of Mathematics and Computer Science, Freie Universität Berlin, 14195 Berlin, Germany

²⁾Department of Chemistry, Stanford University, Stanford, CA, 94305, USA

We illustrate relationships between classical kernel-based dimensionality reduction techniques and eigendecompositions of empirical estimates of *reproducing kernel Hilbert space* (RKHS) operators associated with dynamical systems. In particular, we show that kernel *canonical correlation analysis* (CCA) can be interpreted in terms of kernel transfer operators and that coherent sets of particle trajectories can be computed by applying kernel CCA to Lagrangian data. We demonstrate the efficiency of this approach with several examples, namely the well-known Bickley jet, ocean drifter data, and a molecular dynamics problem with a time-dependent potential. Furthermore, we propose a straightforward generalization of *dynamic mode decomposition* (DMD) called *coherent mode decomposition* (CMD).

I. INTRODUCTION

Over the last years, several kernel-based methods for the analysis of high-dimensional data sets have been developed, many of which can be seen as nonlinear extensions of classical linear methods, e.g., kernel *principal component analysis* (PCA)^{1,2}, kernel *canonical correlation analysis* (CCA)^{3,4}, and kernel *time-lagged independent component analysis* (TICA)^{5,6}. The basic idea behind these methods is to represent data by elements in reproducing kernel Hilbert spaces associated with positive definite kernels. These methods can be used for classification, feature extraction, clustering, or dimensionality reduction^{2,7,8}.

The main goal of this work is to establish connections between machine learning and dynamical systems theory. While the intended applications might differ, the resulting approaches and algorithms often share many similarities. Relationships between kernel embeddings of conditional probability distributions^{9,10} and transfer operators such as the Perron–Frobenius and Koopman operators^{11,12} have recently been detailed in Ref. 13. Furthermore, it has been shown that eigenfunctions of empirical estimates of these operators can be obtained by solving an auxiliary matrix eigenvalue problem. The eigenfunctions of transfer operators encode important global properties of the underlying dynamical system, which can, for instance, be used to detect metastable sets. Other applications include model reduction and control^{14,15}, which we will, however, not consider here. Metastability is related to the existence of a spectral gap: for short time scales, the system appears to be equilibrated, but actually explores the state space of the system only locally; at long time scales, however, there are rare transitions between such metastable states¹⁶. In the molecular dynamics context, for example, metastable states correspond

to different conformations of molecules. We now want to extend this framework to so-called *coherent sets*—a generalization of metastable sets to nonautonomous and aperiodic systems¹⁷—, which again can be regarded as eigenfunctions of certain operators associated with a dynamical system. Coherent sets are regions of the state space that are not dispersed over a specific time interval. That is, if we let the system evolve, elements of a coherent set will, with a high probability, stay close together, whereas other regions of the state space might be distorted entirely.

There is an abundance of publications on the numerical approximation of coherent sets, which we will not review in detail here (see, e.g., Refs. 17–22 and references therein). A comparison of approaches for Lagrangian data, which we mainly consider here, can be found in Ref. 23. Furthermore, we will not address the problem of possibly sparse or incomplete data. Our goal is to illustrate relationships with established kernel-based approaches and to show that existing methods—developed independently and with different applications in mind, predating many algorithms for the computation of finite-time coherent sets—can be directly applied to detect coherent sets in Lagrangian data. Comparisons to some recently proposed singular value decomposition approaches are presented in Appendix A, and potential improvements and generalizations of these methods will be considered in future work.

In this work, we show that kernel CCA, when applied to dynamical data, admits a natural interpretation in terms of kernel transfer operators and that the resulting eigenvalue problems are directly linked to methods for the computation of coherent sets. In Section II, we will briefly introduce transfer operators and review the notion of positive definite kernels and induced Hilbert spaces as well as nonlinear generalizations of covariance and cross-covariance matrices. We will then define empirical RKHS operators and show that diverse algorithms can be formulated as eigenvalue problems involving such operators. The relationships between kernel CCA and coherent sets will be studied in Section III. Furthermore, we will propose a method called *coherent mode decom-*

^{a)}stefan.klus@fu-berlin.de

^{b)}bhusic@stanford.edu

^{c)}mattes.mollenhauer@fu-berlin.de

position, which can be seen as a combination of CCA and DMD^{15,24,25}. Section IV contains numerical results illustrating how to use the presented kernel-based methods for the analysis of dynamical systems. We conclude with a summary of the main results and open problems in Section V.

II. PREREQUISITES

We will only briefly introduce transfer operators, reproducing kernel Hilbert spaces, and operators mapping from one such space to another one (or itself). For more details on the properties of these spaces and the introduced operators, we refer the reader to Refs. 2, 7, and 8 and Refs. 13, 26, and 27, respectively.

A. Transfer operators

Let $\{X_t\}_{t \geq 0}$ be a stochastic process defined on the state space $\mathbb{X} \subset \mathbb{R}^d$ and let τ be a fixed lag time. We assume that there exists a *transition density function* $p_\tau: \mathbb{X} \times \mathbb{X} \rightarrow \mathbb{R}$ such that $p_\tau(y | x)$ is the probability of $X_{t+\tau} = y$ given $X_t = x$. Given $1 \leq r \leq \infty$, we write $L^r(\mathbb{X})$ for the standard space of r -Lebesgue integrable functions on \mathbb{X} . Then, for a probability density μ on \mathbb{X} , let $L_\mu^r(\mathbb{X})$ denote the spaces of r -integrable functions with respect to the corresponding probability measure induced by the density μ ; that is, $\|f\|_{L_\mu^r(\mathbb{X})}^r = \int |f(x)|^r \mu(x) dx$.

Given a probability density $p \in L^1(\mathbb{X})$ and an observable $f \in L^\infty(\mathbb{X})$, we define the *Perron–Frobenius operator* $\mathcal{P}: L^1(\mathbb{X}) \rightarrow L^1(\mathbb{X})$ and the *Koopman operator* $\mathcal{K}: L^\infty(\mathbb{X}) \rightarrow L^\infty(\mathbb{X})$ by

$$\begin{aligned} (\mathcal{P}p)(y) &= \int p_\tau(y | x) p(x) dx, \\ (\mathcal{K}f)(x) &= \int p_\tau(y | x) f(y) dy. \end{aligned}$$

Assuming the process admits a unique equilibrium density π , i.e., $\mathcal{P}\pi = \pi$, we can define for $u = \pi(x)^{-1} p(x)$ the *Perron–Frobenius operator with respect to the equilibrium density* $\mathcal{T}: L_\pi^1(\mathbb{X}) \rightarrow L_\pi^1(\mathbb{X})$ as

$$(\mathcal{T}u)(y) = \frac{1}{\pi(y)} \int p_\tau(y | x) \pi(x) u(x) dx.$$

Under certain conditions, these transfer operators can be defined on $L^r(\mathbb{X})$ and $L_\pi^r(\mathbb{X})$ for other choices of r . From now on, we will always assume that they are well-defined for $r = 2$ (see Refs. 12, 28, and 29 for details). This is common whenever Hilbert space properties are needed in the context of transfer operators.

Remark II.1. For time-homogeneous systems, the associated transfer operators depend only on the lag time τ . If the system is time-inhomogeneous, on the other hand, the lag time is not sufficient to parametrize the evolution

of the system since it also depends on the starting time. This is described in detail in Ref. 30. The transition density and the operators thus require two parameters; however, we will omit the starting time dependence for the sake of clarity.

B. Reproducing kernel Hilbert spaces

Given a set \mathbb{X} and a space \mathbb{H} of functions $f: \mathbb{X} \rightarrow \mathbb{R}$, \mathbb{H} is called a *reproducing kernel Hilbert space (RKHS)* with inner product $\langle \cdot, \cdot \rangle_{\mathbb{H}}$ if there exists a function $k: \mathbb{X} \times \mathbb{X} \rightarrow \mathbb{R}$ with the following properties:

- (i) $\langle f, k(x, \cdot) \rangle_{\mathbb{H}} = f(x)$ for all $f \in \mathbb{H}$, and
- (ii) $\mathbb{H} = \overline{\text{span}\{k(x, \cdot) \mid x \in \mathbb{X}\}}$.

The function k is called a *kernel* and the first property above the *reproducing property*. A direct consequence is that $\langle k(x, \cdot), k(x', \cdot) \rangle_{\mathbb{H}} = k(x, x')$. That is, the map $\phi: \mathbb{X} \rightarrow \mathbb{H}$ given by $x \mapsto k(x, \cdot)$ can be regarded as a feature map associated with x , the so-called *canonical feature map*^a. It is thus possible to represent data by functions in the RKHS. Frequently used kernels include the polynomial kernel and the Gaussian kernel, given by $k(x, x') = (c + x^\top x')^p$ and $k(x, x') = \exp(-\|x - x'\|_2^2/2\sigma^2)$, respectively. While the feature space associated with the polynomial kernel is finite-dimensional, the feature space associated with the Gaussian kernel is infinite-dimensional; see, e.g., Ref. 8. Inner products in these spaces, however, are not evaluated explicitly, but only implicitly through kernel evaluations. This is one of the main advantages of kernel-based methods^{1,7}. Algorithms that can be purely expressed in terms of inner product evaluations can thus be easily *kernelized*, resulting, as described above, in nonlinear extensions of methods such as PCA, CCA, or TICA.

C. Covariance operators and Gram matrices

Let (X, Y) be a random variable on $\mathbb{X} \times \mathbb{Y}$, where $\mathbb{X} \subset \mathbb{R}^{d_x}$ and $\mathbb{Y} \subset \mathbb{R}^{d_y}$. The dimensions d_x and d_y can in principle be different. For our applications, however, the spaces \mathbb{X} and \mathbb{Y} are often identical. The associated marginal distributions are denoted by $\mathbb{P}_x(X)$ and $\mathbb{P}_y(Y)$, the joint distribution by $\mathbb{P}(X, Y)$, and the corresponding densities—which we assume exist—by $p_x(x)$, $p_y(y)$, and $p(x, y)$, respectively. Furthermore, let k and l be the kernels associated with \mathbb{X} and \mathbb{Y} and ϕ and ψ the respective feature maps. We will always assume that requirements

^a Such a feature map $\phi: \mathbb{X} \rightarrow \mathbb{H}$ admitting the property $k(x, x') = \langle \phi(x), \phi(x') \rangle_{\mathbb{H}}$ is not uniquely defined. There are other feature space representations such as, for instance, the Mercer feature space^{2,8,31}. As long as we are only interested in kernel evaluations, however, it does not matter which one is considered.

such as measurability of the kernels and feature maps as well as separability of the RKHSs are satisfied.^b The RKHSs induced by the kernels k and l are denoted by \mathbb{H}_x and \mathbb{H}_y .

We will now introduce covariance operators and cross-covariance operators^{26,27} on RKHSs. In what follows, we will always assume that $\mathbb{E}_x[k(X, X)] < \infty$ and $\mathbb{E}_y[l(Y, Y)] < \infty$, which ensures that these operators are well-defined and Hilbert–Schmidt (for a comprehensive overview of kernel covariance operators and their applications, see Ref. 10 and references therein). For any $f \in \mathbb{H}_x$, let

$$\psi(Y) \otimes \phi(X): f \mapsto \psi(Y) \langle \phi(X), f \rangle_{\mathbb{H}_x}$$

denote the *tensor product operator*³² from \mathbb{H}_x to \mathbb{H}_y defined by $\phi(X)$ and $\psi(Y)$.

Definition II.2 (Covariance operators). *The covariance operator $\mathcal{C}_{xx}: \mathbb{H}_x \rightarrow \mathbb{H}_x$ and the cross-covariance operator $\mathcal{C}_{yx}: \mathbb{H}_x \rightarrow \mathbb{H}_y$ are defined as*

$$\begin{aligned} \mathcal{C}_{xx} &:= \int \phi(X) \otimes \phi(X) d\mathbb{P}(X) = \mathbb{E}_x[\phi(X) \otimes \phi(X)], \\ \mathcal{C}_{yx} &:= \int \psi(Y) \otimes \phi(X) d\mathbb{P}(Y, X) = \mathbb{E}_{yx}[\psi(Y) \otimes \phi(X)]. \end{aligned}$$

Kernel covariance operators satisfy

$$\langle g, \mathcal{C}_{yx} f \rangle_{\mathbb{H}_y} = \text{Cov}[g(Y), f(X)]$$

for all $f \in \mathbb{H}_x$, $g \in \mathbb{H}_y$. Defining $\phi_c(X) = \phi(X) - \mathbb{E}_x[\phi(X)]$ and $\psi_c(Y) = \psi(Y) - \mathbb{E}_y[\psi(Y)]$, the corresponding centered counterparts of the covariance and cross-covariance operators \mathcal{C}_{xx} and \mathcal{C}_{yx} are defined in terms of the mean-subtracted feature maps.

As these operators can in general not be determined analytically, empirical estimates are computed from data, i.e.,

$$\begin{aligned} \hat{\mathcal{C}}_{xx} &= \frac{1}{n} \sum_{i=1}^n \phi(x_i) \otimes \phi(x_i) = \frac{1}{n} \Phi \Phi^\top, \\ \hat{\mathcal{C}}_{yx} &= \frac{1}{n} \sum_{i=1}^n \psi(y_i) \otimes \phi(x_i) = \frac{1}{n} \Psi \Phi^\top, \end{aligned} \tag{1}$$

where $\Phi = [\phi(x_1), \dots, \phi(x_n)]$ and $\Psi = [\psi(y_1), \dots, \psi(y_n)]$ and the training data $\{(x_i, y_i)\}_{i=1}^n$ is drawn i.i.d. from $\mathbb{P}(X, Y)$. Analogously, the mean-subtracted feature maps can be used to obtain empirical estimates of the centered operators. Since in practice we often cannot explicitly deal with these operators, in particular if the feature space is infinite-dimensional, we seek to reformulate algorithms in terms of Gram matrices.

Definition II.3 (Gram matrices). *Given training data as defined above, the Gram matrices $G_{xx}, G_{yy} \in \mathbb{R}^{n \times n}$ are defined as*

$$\begin{aligned} G_{xx} &= \Phi^\top \Phi = [k(x_i, x_j)]_{i,j=1}^n, \\ G_{yy} &= \Psi^\top \Psi = [l(y_i, y_j)]_{i,j=1}^n. \end{aligned}$$

For a Gram matrix G , its centered version \tilde{G} is defined by $\tilde{G} = N_0 G N_0$, where $N_0 = I - \frac{1}{n} \mathbf{1} \mathbf{1}^\top$ and $\mathbf{1} \in \mathbb{R}^n$ is a vector composed of ones⁴. Note that centered Gram matrices are not regular.

Remark II.4. In what follows, if not noted otherwise, we assume that the covariance operators \mathcal{C}_{xx} and \mathcal{C}_{yy} and the Gram matrices G_{xx} and G_{yy} are properly centered for CCA.

D. Kernel transfer operators

We now show how transfer operators can be written in terms of covariance and cross-covariance operators—this leads to the concept of *kernel transfer operators*. Note that we assume the Perron–Frobenius operator and the Koopman operator to be well-defined on $L^2(\mathbb{X})$ as discussed in Section II A. Kernel transfer operators follow from the assumption that densities and observables in $L^2(\mathbb{X})$ can be represented as elements of the RKHS \mathbb{H}_x . Under some technical requirements, such as $\int_{\mathbb{X}} k(x, x) dx = \int_{\mathbb{X}} \|\phi(x)\|_{\mathbb{H}_x}^2 dx < \infty$, the elements of \mathbb{H}_x are included in $L^2(\mathbb{X})$ when they are identified with the respective equivalence class of square integrable functions. This correspondence can be derived from the theory of $L^2(\mathbb{X})$ integral operators⁸ and is often used in statistical learning theory³³. We may therefore assume that we can identify RKHS elements with the corresponding equivalence classes of functions in $L^2(\mathbb{X})$. By requiring $\mathbb{E}_\mu[k(X, X)] < \infty$ for a probability density $\mu(x)$, we obtain a similar statement for $L_\mu^2(\mathbb{X})$.

We refer to Ref. 13 for the derivation of kernel transfer operators and a description of their relationships with kernel embeddings of conditional distributions. We will omit the technical details and directly define kernel transfer operators as the RKHS analogue of the standard transfer operators defined in Section II A. Using the same integral representations as before and defining the transfer operators on \mathbb{H}_x instead of $L^2(\mathbb{X})$, we obtain the *kernel Perron–Frobenius operator* $\mathcal{P}_k: \mathbb{H}_x \rightarrow \mathbb{H}_x$ and the *kernel Koopman operator* $\mathcal{K}_k: \mathbb{H}_x \rightarrow \mathbb{H}_x$, respectively.

By defining the time-lagged process $Y_t = X_{t+\tau}$, we can write kernel transfer operators in terms of covariance and cross-covariance operators¹³. Note that X_t and Y_t are defined on the same state space \mathbb{X} ; therefore, we have $\mathbb{H}_x = \mathbb{H}_y$ and hence $\mathcal{C}_{yx}: \mathbb{H}_x \rightarrow \mathbb{H}_x$ in this special case. We obtain the important properties $\mathcal{C}_{xx} \mathcal{P}_k g = \mathcal{C}_{yx} g$ and $\mathcal{C}_{xx} \mathcal{K}_k g = \mathcal{C}_{xy} g$ for all $g \in \mathbb{H}_x$, which allows us to write

$$\begin{aligned} \mathcal{P}_k &= (\mathcal{C}_{xx} + \varepsilon \mathcal{I})^{-1} \mathcal{C}_{yx}, \\ \mathcal{K}_k &= (\mathcal{C}_{xx} + \varepsilon \mathcal{I})^{-1} \mathcal{C}_{xy}. \end{aligned} \tag{2}$$

^b In most cases, these properties follow from mild assumptions about \mathbb{X} and \mathbb{Y} . For an in-depth discussion of these technical details, see Ref. 8.

Here, $(\mathcal{C}_{xx} + \varepsilon\mathcal{I})^{-1}$ is the Tikhonov-regularized inverse of \mathcal{C}_{xx} with regularization parameter $\varepsilon > 0$.^c Note the abuse of notation, since equality in the above inverse problems is only given asymptotically for $\varepsilon \rightarrow 0$ and pointwise for feasible $\mathcal{C}_{yx}g \in \mathbb{H}_x$. Since \mathcal{C}_{xx} is a compact operator, it does not admit a globally defined bounded inverse if the RKHS is infinite-dimensional. However, $(\mathcal{C}_{xx} + \varepsilon\mathcal{I})^{-1}$ always exists and is bounded. In fact, the operators \mathcal{P}_k and \mathcal{K}_k as given in the regularized form above are Hilbert–Schmidt.

The above notation and regularization of inverse covariance operators is standard in the context of kernel embeddings of conditional distributions and related Bayesian learning techniques. We refer to Refs. 9, 10, 37–39 for detailed discussions of properties of this ill-posed inverse problem in specific applications.

By replacing the analytical covariance operators with their empirical estimates in (2), we obtain empirical estimates for kernel transfer operators¹³. As done with empirical covariance operators in (1), it is possible to rewrite the empirical estimates of kernel transfer operators in terms of RKHS features in Φ and Ψ (see Refs. 10 and 13 for the derivation):

$$\begin{aligned}\hat{\mathcal{P}}_k &= (\hat{\mathcal{C}}_{xx} + \varepsilon\mathcal{I})^{-1}\hat{\mathcal{C}}_{yx} \\ &= \Psi(G_{xy}^{-1}(G_{xx} + n\varepsilon I)^{-1}G_{xy})\Phi^\top, \\ \hat{\mathcal{K}}_k &= (\hat{\mathcal{C}}_{xx} + \varepsilon\mathcal{I})^{-1}\hat{\mathcal{C}}_{xy} \\ &= \Phi(G_{xx} + n\varepsilon I)^{-1}\Psi^\top.\end{aligned}\quad (3)$$

Note that now Φ and Ψ both contain observations in the same space \mathbb{H}_x , since X_t and Y_t are both defined on \mathbb{X} .

E. Empirical RKHS operators

In what follows, we will consider finite-rank RKHS operators given by a matrix which represents the action of the operator on fixed elements in the RKHSs. We will use this general setting to formulate results about the eigenvalues and eigenfunctions of empirical RKHS operators. Given a matrix $B \in \mathbb{R}^{n \times n}$, we define the bounded finite-rank operator $\hat{\mathcal{S}}: \mathbb{H}_x \rightarrow \mathbb{H}_y$ by

$$\hat{\mathcal{S}} = \Psi B \Phi^\top = \sum_{i,j=1}^n b_{ij} \psi(y_i) \otimes \phi(x_j). \quad (4)$$

We remark that although Ψ and Φ may contain infinite-dimensional objects, we express inner products between RKHS elements in the classical matrix-vector multiplication form. That is, we interpret the embedded RKHS elements as (potentially infinite-dimensional) column vectors. This notation has become a de-facto standard

in the machine learning community¹⁰. We can write empirical estimates of covariance operators in the form of (4). If the RKHS training features in Φ and Ψ are generated i.i.d. by the joint probability distribution $\mathbb{P}(X, Y)$ of random variables X and Y , then the cross-covariance operator $\hat{\mathcal{C}}_{yx}$ takes the general form of an empirical RKHS operator with $B = \frac{1}{n}I$. We obtain $\hat{\mathcal{C}}_{xx}$ as another special case with identical features $\Psi = \Phi$ drawn only from $\mathbb{P}(X)$. Furthermore, the empirical estimates of the kernel Perron–Frobenius and kernel Koopman operator are special cases of $\hat{\mathcal{S}}$ as seen in (3) with $B = G_{xy}^{-1}(G_{xx} + n\varepsilon I)^{-1}G_{xy}$ and $B = (G_{xx} + n\varepsilon I)^{-1}$, respectively. Note that the roles of Φ and Ψ are interchanged for the empirical estimate of the Koopman operator, i.e., it is of the form $\hat{\mathcal{S}} = \Phi B \Psi^\top$.

We now show how spectral decomposition techniques can be applied to empirical RKHS operators in this general setting.^d We can compute eigenvalues and corresponding eigenfunctions of $\hat{\mathcal{S}}$ by solving auxiliary matrix eigenvalue problems. For the sake of self-containedness, we briefly reproduce the eigendecomposition result from Ref. 13.

Proposition II.5. *Suppose Φ and Ψ contain linearly independent elements. Let $\hat{\mathcal{S}} = \Psi B \Phi^\top$, then*

(i) $\hat{\mathcal{S}}$ has an eigenvalue $\lambda \neq 0$ with corresponding eigenfunction $\varphi = \Psi v$ if and only if v is an eigenvector of $B G_{xy}$ associated with λ , and, similarly,

(ii) $\hat{\mathcal{S}}$ has an eigenvalue $\lambda \neq 0$ with corresponding eigenfunction $\varphi = \Phi G_{xx}^{-1}v$ if and only if v is an eigenvector of $G_{xy} B$.

Note that for the Gaussian kernel, linear independence of elements in Φ and Ψ reduces to requiring that the training data contains pairwise distinct elements in \mathbb{X} and \mathbb{Y} , respectively. For dynamical systems applications, we typically assume that Φ and Ψ contain information about the system at time t and at time $t + \tau$, respectively. A more detailed version of Proposition II.5 and its extension to the singular value decomposition are described in Ref. 40. Further properties of $\hat{\mathcal{S}}$ and its decompositions will be studied in future work. Note that we generally assume that empirical estimates of RKHS operators converge in probability to their analytical counterparts in operator norm in the infinite data limit. These statistical properties and the resulting associated spectral convergence are examined in for example in Ref. 33.

^c See Refs. 34–36 for a detailed discussion of ill-posed inverse problems and the regularization of bounded linear operators on Hilbert spaces.

^d In general, all considered kernel transfer operators in this paper are compositions of compact and bounded operators and therefore compact. They admit series representations in terms of singular value decompositions as well as eigendecompositions in the self-adjoint case³². The functional analytic details and the convergence of $\hat{\mathcal{S}}$ and its spectral properties in the infinite-data limit depend on the specific scenario and are beyond the scope of this paper.

F. Applications of RKHS operators

Decompositions of RKHS operators have diverse applications, which we will only touch upon here. We will consider a specific problem—namely, kernel CCA—in Section III.

(a) By sampling points from the uniform distribution, the *Mercer feature map*^{2,8,31} with respect to the Lebesgue measure on \mathbb{X} can be approximated by computing eigenfunctions of $\widehat{\mathcal{C}}_{xx}$ —i.e., $B = \frac{1}{n}I$ and the auxiliary matrix eigenvalue problem is $\frac{1}{n}G_{xx}v = \lambda v$ —as shown in Ref. 40. This can be easily extended to other measures.

(b) Similarly, given an arbitrary data set $\{x_i\}_{i=1}^n$, kernel PCA computes the eigenvectors corresponding to the largest eigenvalues of the centered Gram matrix G_{xx} and defines these eigenvectors as the data points projected onto the respective principal components. It is well-known that kernel PCA can also be defined in terms of the centered covariance operator $\widehat{\mathcal{C}}_{xx}$. A detailed connection of the spectrum of the Gram matrix and the covariance operator is given in Ref. 41. Up to scaling, the eigenfunctions evaluated in the data points correspond to the principal components.

(c) Given training data $x_i \sim p_x$ and $y_i = \Theta^\tau(x_i)$, where Θ denotes the flow associated with the dynamical system and τ the lag time—that is, if x_i is the state of the system at time t , then y_i is the state of the system at time $t + \tau$ —, we define Φ and Ψ as above. Eigenvalues and eigenfunctions of kernel transfer operators can be computed by solving a standard matrix eigenvalue problem (see Proposition II.5). Eigendecompositions of these operators result in metastable sets. For more details and real-world examples, see Refs. 13 and 42. The main goal of this paper is the extension of the aforementioned methods to compute *coherent sets* instead of *metastable sets*.

III. KERNEL CCA AND COHERENT SETS

Given two multidimensional random variables X and Y , standard CCA finds two sets of basis vectors such that the correlations between the projections of X and Y onto these basis vectors are maximized⁴³. The new bases can be found by computing the dominant eigenvalues and corresponding eigenvectors of a matrix composed of covariance and cross-covariance matrices. Just like kernel PCA is a nonlinear extension of PCA, kernel CCA is a generalization of CCA. The goal of kernel CCA is to find two *nonlinear* mappings $f(X)$ and $g(Y)$, where $f \in \mathbb{H}_x$ and $g \in \mathbb{H}_y$, such that their correlation is maximized⁴⁴. That is, instead of matrices, kernel CCA is now formulated in terms of covariance and cross-covariance operators. More precisely, the kernel CCA problem can be written as

$$\sup_{\substack{f \in \mathbb{H}_x \\ g \in \mathbb{H}_y}} \langle g, \mathcal{C}_{yx}f \rangle_{\mathbb{H}_y} \quad \text{s.t.} \quad \begin{cases} \langle f, \mathcal{C}_{xx}f \rangle_{\mathbb{H}_x} = 1, \\ \langle g, \mathcal{C}_{yy}g \rangle_{\mathbb{H}_y} = 1, \end{cases}$$

and the solution is given by the eigenfunctions corresponding to the largest eigenvalue of the problem

$$\begin{cases} \mathcal{C}_{yx}f = \rho \mathcal{C}_{yy}g, \\ \mathcal{C}_{xy}g = \rho \mathcal{C}_{xx}f. \end{cases} \quad (5)$$

Further eigenfunctions corresponding to subsequent eigenvalues can be taken into account as in the standard setting described above. In practice, the eigenfunctions are estimated from finite samples. The empirical estimates of f and g are denoted by \hat{f} and \hat{g} , respectively.

Example III.1. In order to illustrate kernel CCA, let us analyze a synthetic data set similar to the one described in Ref. 44 using a Gaussian kernel with bandwidth $\sigma = 0.3$. Algorithms to solve the CCA problem will be described below. The results are shown in Figure 1. Note that classical CCA would not be able to capture the nonlinear relationship between X and Y . \blacktriangle

A. RKHS operator formulation

Since the inverses of the covariance operators in general do not exist, the regularized versions $(\mathcal{C}_{xx} + \varepsilon \mathcal{I})^{-1}$ and $(\mathcal{C}_{yy} + \varepsilon \mathcal{I})^{-1}$ (cf. Section IID) are also typically used in the context of CCA⁴⁴. Solving the first equation in (5) for g and inserting it into the second equation, this results in

$$(\mathcal{C}_{xx} + \varepsilon \mathcal{I})^{-1} \mathcal{C}_{xy} (\mathcal{C}_{yy} + \varepsilon \mathcal{I})^{-1} \mathcal{C}_{yx} f = \rho^2 f. \quad (6)$$

Comparing this with the aforementioned transfer operator representations (2), $(\mathcal{C}_{xx} + \varepsilon \mathcal{I})^{-1} \mathcal{C}_{xy}$ can be interpreted as an approximation of the kernel Koopman operator, and $(\mathcal{C}_{yy} + \varepsilon \mathcal{I})^{-1} \mathcal{C}_{yx}$ as a kernel Koopman operator where now the roles of X and Y are reversed or as a reweighted Perron–Frobenius operator. The composition of these operators corresponds to a push-forward and subsequent pull-back of a density f . Eigenfunctions of the operator whose associated eigenvalues are close to one thus remain nearly unchanged under the forward–backward dynamics. This is closely related to the notion of *coherence* and will be discussed in Section IIIC.

Lemma III.2. *Replacing the covariance and cross-covariance operators by their empirical estimates, the eigenvalue problem (6) can be written as*

$$\Phi B \Phi^\top \hat{f} = \rho^2 \hat{f},$$

with $B = (G_{xx} + n\varepsilon I)^{-1} (G_{yy} + n\varepsilon I)^{-1} G_{yy}$.

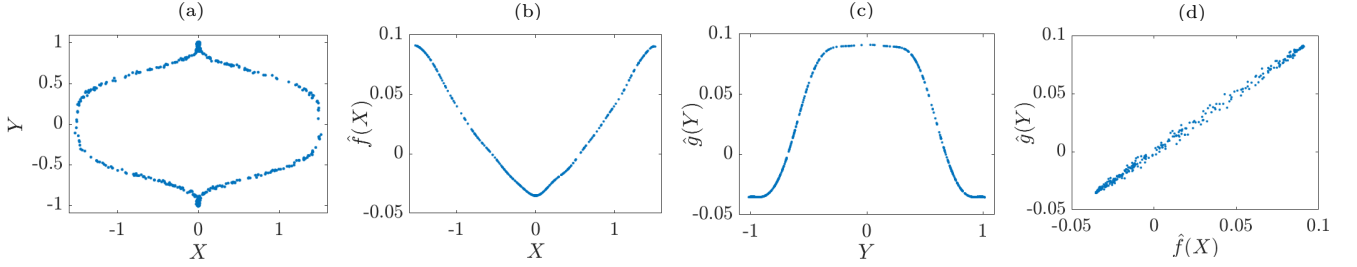


FIG. 1. Kernel CCA applied to noisy generalized superellipse data. The transformed variables $\hat{f}(X)$ and $\hat{g}(Y)$ are clearly highly correlated.

Proof. Inserting the definitions of the empirical covariance and cross-covariance operators yields

$$(\Phi\Phi^\top + n\varepsilon I)^{-1}\Phi\Psi^\top(\Psi\Psi^\top + n\varepsilon I)^{-1}\Psi\Phi^\top\hat{f} = \rho^2\hat{f}.$$

Using $\Psi^\top(\Psi\Psi^\top + n\varepsilon I)^{-1} = (\Psi^\top\Psi + n\varepsilon I)^{-1}\Psi^\top$, see Ref. 10, and a similar identity for Φ concludes the proof. \blacksquare

That is, the empirical RKHS operator for kernel CCA is of the form $\hat{S} = \Phi B \Phi^\top$. Applying Proposition II.5, we must solve the auxiliary problem

- (i) $(G_{xx} + n\varepsilon I)^{-1}(G_{yy} + n\varepsilon I)^{-1}G_{yy}G_{xx}v = \rho^2v$, with $\hat{f} = \Phi v$, or
- (ii) $G_{xx}(G_{xx} + n\varepsilon I)^{-1}(G_{yy} + n\varepsilon I)^{-1}G_{yy}v = \rho^2v$, with $\hat{f} = \Phi(G_{xx} + n\varepsilon I)^{-1}v$.

Since G_{xx} and $(G_{xx} + n\varepsilon I)^{-1}$ as well as G_{yy} and $(G_{yy} + n\varepsilon I)^{-1}$ commute, the first problem can be equivalently rewritten as $(G_{xx} + n\varepsilon I)^{-1}G_{yy}(G_{yy} + n\varepsilon I)^{-1}G_{xx}v = \rho^2v$ and the second as $(G_{xx} + n\varepsilon I)^{-1}G_{xx}G_{yy}(G_{yy} + n\varepsilon I)^{-1}v = \rho^2v$. The eigenfunction associated with the largest eigenvalue solves the CCA problem, but in order to detect coherent sets, we will need more eigenfunctions later. To obtain the function g corresponding to ρ , we compute

- (i) $\hat{g} = \frac{1}{\rho}\Psi(G_{yy} + n\varepsilon I)^{-1}G_{xx}v$, or
- (ii) $\hat{g} = \frac{1}{\rho}\Psi(G_{yy} + n\varepsilon I)^{-1}G_{xx}(G_{xx} + n\varepsilon I)^{-1}v$.

Algorithm III.3. The CCA problem can be solved as follows:

1. Choose a kernel k and regularization ε .
2. Compute the centered gram matrices G_{xx} and G_{yy} .
3. Solve $G_{xx}(G_{xx} + n\varepsilon I)^{-1}(G_{yy} + n\varepsilon I)^{-1}G_{yy}v = \rho^2v$.

The corresponding eigenfunction \hat{f} evaluated at all data points x_1, \dots, x_n , denoted by \hat{f}_X , is then approximately given by the vector v . We can evaluate the eigenfunctions at any other point as described above, but we

will mainly use the eigenfunction evaluations at the sampled data points for clustering into coherent sets.

Algorithm III.3 is based on the second problem formulation, i.e., item (ii) above. However, the first variant can be used in the same way. Alternatively, we can rewrite it as an eigenvalue problem of the form

$$\begin{cases} (G_{yy} + n\varepsilon I)^{-1}G_{xx}v = \rho w, \\ (G_{xx} + n\varepsilon I)^{-1}G_{yy}w = \rho v, \end{cases}$$

and, consequently,

$$\begin{bmatrix} 0 & G_{yy} \\ G_{xx} & 0 \end{bmatrix} \begin{bmatrix} v \\ w \end{bmatrix} = \rho \begin{bmatrix} (G_{xx} + n\varepsilon I) & 0 \\ 0 & (G_{yy} + n\varepsilon I) \end{bmatrix} \begin{bmatrix} v \\ w \end{bmatrix}. \quad (7)$$

Other formulations can be derived in a similar fashion. The advantage is that no matrices have to be inverted. However, the size of the eigenvalue problem doubles, which might be problematic if the number data points n is large.

The generalized eigenvalue problem (7) is almost identical to the one derived in Ref. 4, with the difference that regularization is applied in a slightly different way. That is, the direct eigendecomposition of RKHS operators as proposed in Ref. 13 results, as expected, in variants of kernel CCA. The statistical convergence of kernel CCA, showing that finite sample estimators converge to the corresponding population counterparts, has been established in Ref. 44. Kernel CCA can be extended to more than two variables or views of the data as described in Refs. 4 and 7, which might also have relevant applications in the dynamical systems context.

B. Finite-dimensional feature space

If the state spaces of the kernels k and l are finite-dimensional, we can directly solve the eigenvalue problem (5) or (6). Assuming the feature space of the kernel k is r_x -dimensional and spanned by the basis functions $\{\phi_1, \dots, \phi_{r_x}\}$, we define $\phi: \mathbb{X} \rightarrow \mathbb{R}^{r_x}$ by $\phi(x) = [\phi_1(x), \dots, \phi_{r_x}(x)]^\top$. That is, we are now using an explicit feature space representation. This induces a ker-

nel by defining $k(x, x') = \langle \phi(x), \phi(x') \rangle$.^e We could, for instance, select a set of radial basis functions, monomials, or trigonometric functions. Analogously, we define a vector-valued function $\psi: \mathbb{Y} \rightarrow \mathbb{R}^{r_y}$, with $\psi(y) = [\psi_1(y), \dots, \psi_{r_y}(y)]^\top$, where r_y is the dimension of the feature space of the kernel l . Any function in the respective RKHS can be written as $f = \alpha^\top \phi$ and $g = \beta^\top \psi$, where $\alpha \in \mathbb{R}^{r_x}$ and $\beta \in \mathbb{R}^{r_y}$ are coefficient vectors.

Given training data $\{(x_i, y_i)\}_{i=1}^n$ drawn from the joint probability distribution, we obtain $\Phi \in \mathbb{R}^{r_x \times n}$ and $\Psi \in \mathbb{R}^{r_y \times n}$ and can compute the centered covariance and cross-covariance matrices $\hat{\mathcal{C}}_{xx}$, $\hat{\mathcal{C}}_{xy}$, and $\hat{\mathcal{C}}_{yy}$ explicitly.

Algorithm III.4. Given explicit feature maps, we obtain the following CCA algorithm:

1. Select basis functions ϕ and ψ and regularization ε .
2. Compute (cross-)covariance matrices $\hat{\mathcal{C}}_{xx}$, $\hat{\mathcal{C}}_{xy}$, $\hat{\mathcal{C}}_{yx}$, and $\hat{\mathcal{C}}_{yy}$.
3. Solve the eigenvalue problem $(\hat{\mathcal{C}}_{xx} + \varepsilon \mathcal{I})^{-1} \hat{\mathcal{C}}_{xy} (\hat{\mathcal{C}}_{yy} + \varepsilon \mathcal{I})^{-1} \hat{\mathcal{C}}_{yx} v = \rho^2 v$.

The eigenfunctions are then given by $\hat{f}(x) = \langle v, \phi(x) \rangle$. Expressions for \hat{g} can be derived analogously.

Remark III.5. Defining $v = (\hat{\mathcal{C}}_{xx} + \varepsilon \mathcal{I})^{-1/2} \tilde{v}$, the eigenvalue problem in Algorithm III.4 becomes

$$(\hat{\mathcal{C}}_{xx} + \varepsilon \mathcal{I})^{-1/2} \hat{\mathcal{C}}_{xy} (\hat{\mathcal{C}}_{yy} + \varepsilon \mathcal{I})^{-1} \hat{\mathcal{C}}_{yx} (\hat{\mathcal{C}}_{xx} + \varepsilon \mathcal{I})^{-1/2} \tilde{v} = \rho^2 \tilde{v}.$$

The transformed eigenvectors \tilde{v} are thus equivalent to the right singular vectors of the matrix

$$(\hat{\mathcal{C}}_{yy} + \varepsilon \mathcal{I})^{-1/2} \hat{\mathcal{C}}_{yx} (\hat{\mathcal{C}}_{xx} + \varepsilon \mathcal{I})^{-1/2}$$

and the values ρ are given by the singular values, which we assume to be sorted in nonincreasing order. Setting $\varepsilon = 0$, this is equivalent to the approach proposed in Ref. 30, where the estimated covariance and cross-covariance matrices are by definition regular.^f Regularity can be achieved by removing redundant basis functions. More details are discussed in Appendix A.

The difference between the Gram matrix approach described in Section III A and the algorithm proposed here is that the size of the eigenvalue problem associated with the former depends on the number of data points and permits the dimension of the feature space to be infinite-dimensional, whereas the eigenvalue problem associated with the latter depends on the dimension

of the feature space but not on the size of the training data set. This is equivalent to the distinction between *extended dynamic mode decomposition* (EDMD)⁴⁵ and kernel EDMD⁴⁶ (or the variational approach⁴⁷ and kernel TICA⁶, where the system is typically assumed to be reversible; see Ref. 13 for a detailed comparison) with the small difference that often the Moore–Penrose pseudoinverse⁴⁸ is used for EDMD in lieu of the Tikhonov-regularized inverse.

C. Relationships between kernel CCA and transfer operators

We have seen in Section III A that the resulting eigenvalue problem (6) involves expressions resembling kernel transfer operators. The goal now is illustrate how this eigenvalue problem is related to the operators derived in Ref. 21 for detecting coherent sets. We first introduce a *forward operator* $\mathcal{F}: L_\mu^2(\mathbb{X}) \rightarrow L^2(\mathbb{Y})$ by

$$(\mathcal{F}f)(y) = \int p_\tau(y | x) f(x) \mu(x) dx,$$

where μ is some reference density of interest. Furthermore, let $\nu = \mathcal{F}\mathbf{1}$ be the image density obtained by mapping the indicator function on \mathbb{X} forward in time. Normalizing \mathcal{F} with respect to ν , we obtain a new operator $\mathcal{A}: L_\mu^2(\mathbb{X}) \rightarrow L_\nu^2(\mathbb{Y})$ and its adjoint $\mathcal{A}^*: L_\nu^2(\mathbb{Y}) \rightarrow L_\mu^2(\mathbb{X})$, with

$$\begin{aligned} (\mathcal{A}f)(y) &= \int \frac{p_\tau(y | x)}{\nu(y)} f(x) \mu(x) dx, \\ (\mathcal{A}^*g)(x) &= \int p_\tau(y | x) g(y) dy. \end{aligned}$$

It holds that $\langle \mathcal{A}f, g \rangle_\nu = \langle f, \mathcal{A}^*g \rangle_\mu$. Consequently, \mathcal{A} plays the role of a reweighted Perron–Frobenius operator, whereas \mathcal{A}^* can be interpreted as an analogue of the Koopman operator (note that \mathcal{A} and \mathcal{A}^* are defined on reweighted L^2 -spaces). A more detailed derivation can be found in Ref. 21, where the operator $\mathcal{A}^* \mathcal{A}$ (or a trajectory-averaged version thereof) is used to detect coherent sets. We want to show that this is, up to regularization, equivalent to the operator in (6).

Proposition III.6. *Assuming that $\mathcal{A}f \in \mathbb{H}_Y$ for all $f \in \mathbb{H}_X$, it holds that $\mathcal{C}_{YY} \mathcal{A}f = \mathcal{C}_{YX} f$.*

Proof. The proof is almost identical to the proof for the standard Perron–Frobenius operator (see Ref. 13). For all $g \in \mathbb{H}_Y$, we obtain

$$\begin{aligned} \langle \mathcal{C}_{YY} \mathcal{A}f, g \rangle_{\mathbb{H}_Y} &= \mathbb{E}_Y [\mathcal{A}f(Y) g(Y)] \\ &= \iint \frac{p(y | x)}{\nu(y)} f(x) \mu(x) dx g(y) \nu(y) dy \\ &= \iint p(y | x) f(x) g(y) \mu(x) dx dy \end{aligned}$$

^e For the Mercer feature space representation^{2,31} the functions form an orthogonal basis, but orthogonality is not required here.

^f Note that their notation is slightly different: $C_{00} \triangleq \hat{\mathcal{C}}_{xx}$, $C_{11} \triangleq \hat{\mathcal{C}}_{yy}$, but $C_{01} \triangleq \hat{\mathcal{C}}_{yx}$.

$$\begin{aligned}
&= \iint p(x, y) f(x) g(y) dx dy \\
&= \mathbb{E}_{X,Y} [f(X) g(Y)] \\
&= \langle \mathcal{C}_{YX} f, g \rangle_{\mathbb{H}_Y}.
\end{aligned}
\quad \blacksquare$$

We define the RKHS approximation of the operator \mathcal{A} by $\mathcal{A}_k = (\mathcal{C}_{YY} + \varepsilon I)^{-1} \mathcal{C}_{YX}$. Note that the operator technically depends not only on k but also on l , which we omit for brevity. In practice, we typically use the same kernel for \mathbb{X} and \mathbb{Y} . As a result, the eigenvalue problem (6) can now be written as

$$\mathcal{K}_k \mathcal{A}_k f = \rho^2 f.$$

The adjointness property for $\varepsilon = 0$, i.e., assuming that the inverse exists without regularization^g, can be verified as follows:

$$\langle \mathcal{A}_k f, g \rangle_\nu = \langle \mathcal{C}_{YX} f, g \rangle_{\mathbb{H}_Y} = \langle f, \mathcal{C}_{XY} g \rangle_{\mathbb{H}_X} = \langle f, \mathcal{K}_k g \rangle_\mu.$$

We have thus shown that the eigenvalue problem for the computation of coherent sets and the CCA eigenvalue problem are equivalent, provided that the RKHS is an invariant subspace of \mathcal{T}_k . Although this is in general not the case—depending on the kernel the RKHS might be low-dimensional (e.g., for a polynomial kernel), but could also be infinite-dimensional and isometrically isomorphic to L^2 (e.g., for the Gaussian kernel)—, we can use the kernel-based formulation as an approximation and solve it numerically to obtain coherent sets. This is the mathematical justification for the claim that CCA detects coherent sets, which will be corroborated by numerical results in Section IV.

D. Coherent mode decomposition

Borrowing ideas from *dynamic mode decomposition* (DMD)^{24,25}, we now introduce a method that approximates eigenfunctions or eigenmodes of the forward-backward dynamics using linear basis functions and refer to it as *coherent mode decomposition* (CMD)—a mixture of CCA and DMD.^h The relationships between DMD and TICA (including their extensions) and transfer operators are delineated in Refs. 13 and 49. DMD is often used for finding coherent structures in fluid flows, dimensionality reduction, and also prediction and control; see Ref. 15 for an exhaustive analysis and potential applications.

Let us assume we have high-dimensional time-series data but only relatively few snapshots. That is, $\mathbf{X}, \mathbf{Y} \in \mathbb{R}^{d \times n}$ with $d \gg n$, where $\mathbf{X} = [x_1, \dots, x_n]$ and $\mathbf{Y} =$

$[y_1, \dots, y_n]$. This is, for instance, the case for fluid dynamics applications where the, e.g., two- or three-dimensional domain is discretized using (un)structured grids. It is important to note that this analysis is now not based on Lagrangian data as before, where we tracked the positions of particles or drifters over time, but on the Eulerian frame of reference.

Using Algorithm III.4 with $\phi(x) = x$ and $\psi(y) = y$ is infeasible here since the resulting covariance and cross-covariance matrices would be prohibitively large; thus, we apply the kernel-based counterpart. The linear kernel $k: \mathbb{R}^d \times \mathbb{R}^d \rightarrow \mathbb{R}$ is defined by $k(x, x') = \phi(x)^\top \phi(x') = x^\top x'$ and the Gram matrices are simply given by

$$G_{XX} = \mathbf{X}^\top \mathbf{X} \quad \text{and} \quad G_{YY} = \mathbf{Y}^\top \mathbf{Y},$$

where $G_{XX}, G_{YY} \in \mathbb{R}^{n \times n}$.

Algorithm III.7. Coherent mode decomposition.

1. Choose regularization ε .
2. Compute gram matrices G_{XX} and G_{YY} .
3. Solve the eigenvalue problem

$$(G_{XX} + n\varepsilon I)^{-1} (G_{YY} + n\varepsilon I)^{-1} G_{YY} G_{XX} v = \rho^2 v.$$

The eigenfunction \hat{f} evaluated in an arbitrary point $x \in \mathbb{R}^d$ is then given by

$$\begin{aligned}
\hat{f}(x) &= \Phi(x) v = [k(x_1, x), \dots, k(x_n, x)] v = (\mathbf{X}v)^\top x \\
&= \xi^\top \phi(x),
\end{aligned}$$

where we define the *coherent mode* ξ corresponding to the eigenvalue ρ by $\xi = \mathbf{X}v$. That is, ξ contains the coefficients for the basis functions ϕ . Analogously, we obtain

$$\begin{aligned}
\hat{g}(y) &= \frac{1}{\rho} \Psi(y) (G_{YY} + n\varepsilon I)^{-1} G_{XX} v = (\mathbf{Y}w)^\top y \\
&= \eta^\top \psi(y),
\end{aligned}$$

where $w = \frac{1}{\rho} (G_{YY} + n\varepsilon I)^{-1} G_{XX} v$ and $\eta = \mathbf{Y}w$.

As mentioned above, DMD (as a special case of EDMD⁴⁵) typically uses the pseudoinverse to compute matrix representations of the corresponding operators. Nonetheless, a Tikhonov-regularized variant is described in Ref. 50.

IV. NUMERICAL RESULTS

As we have shown above, many dimensionality reduction techniques or methods to analyze high-dimensional data can be regarded as eigendecompositions of certain empirical RKHS operators. We now seek to illustrate how kernel CCA results in coherent sets and potential applications of the coherent mode decomposition.

^g Conditions for the existence of the inverse can be found, for instance, in Ref. 37 and in Section III.B.

^h In fact, the method described below is closer to TICA than DMD, but other variants can be derived in the same fashion, using different combinations of covariance and cross-covariance operators.

A. Coherent sets

We will first apply the method to a well-known benchmark problem, namely the Bickley jet, and then to ocean data and a molecular dynamics problem.

1. Bickley jet

Let us consider a perturbed Bickley jet, which is an approximation of an idealized stratospheric flow⁵¹ and a typical benchmark problem for detecting coherent sets (see, e.g., Refs. 17, 20–22). The flow is illustrated in Figure 2. For a detailed description of the model and its parameters, we refer to Ref. 21. Here, the state space is defined to be periodic in the x_1 -direction with period 20. In order to demonstrate the notion of *coherence*, we arbitrarily color one circular set yellow and one red and observe their evolution. The yellow set is dispersed quickly by the flow; the red set, on the other hand, moves around but barely changes shape. The red set is hence called *coherent*.

We generate 10000 uniformly distributed test points x_i in $\mathbb{X} = [0, 20] \times [-3, 3]$ and then simulate their progression in time. For the computation of the coherent sets, we use only the start and end points of each trajectory, i.e., we define $y_i = \Theta^\tau(x_i)$, where Θ^τ denotes the flow associated with the dynamical system. We set $\tau = 40$. From the vectors x_i and y_i , we then compute the Gram matrices G_{xx} and G_{yy} using the same Gaussian kernel. Here, we define the bandwidth to be $\sigma = 1$ and the regularization parameter to be $\varepsilon = 10^{-7}$.

A few dominant eigenfunctions are shown in Figure 3 (a)–(d). The first eigenfunction distinguishes between the top and bottom “half” and the second one between the middle part and the rest. The subsequent eigenfunctions pick up combinations of the vortices. Applying k -means with $k = 9$ to the dominant eigenfunctions results in the coherent sets shown in Figure 3 (e). This is consistent with the results presented in Ref. 21.

Choosing a finite-dimensional feature space explicitly, as described in Section III B, by selecting a set of radial basis functions whose centers are given by a regular grid leads to comparable results. Currently, only start and end points of trajectories are considered. As a result, points that drift apart and then reunite at time τ would constitute coherent sets. Applying kernel CCA to less well-behaved systems might require more sophisticated kernels that take entire trajectories into account, e.g., by employing averaging techniques as suggested in Ref. 21.

2. Ocean data

Ocean currents are driven by winds and tides, as well as differences in salinity. There are five major gyres as illustrated in Figure 4 (a), which has been reproduced

with permission of the *National Ocean Service* (NOAA).ⁱ Our goal now is to detect these gyres from virtual buoy trajectories. In order to generate Lagrangian data, we use the *OceanParcels* toolbox^j (see Ref. 52 for details) and data from the *GlobCurrent* repository,^k provided by the *European Space Agency*. More precisely, our drifter computations are based on the Eulerian total current at significant wave height from the sum of geostrophic and Ekman current components, starting on the 1st of January 2016 and ending on the 31st of December 2016 with 3-hourly updates.

We place 15000 uniformly distributed virtual drifters in the oceans and let the flow evolve for one year, which thus constitutes the lag time τ . Let x_i denote the initial positions and y_i the new positions of the drifters after one year. The domain is $\mathbb{X} = [-180^\circ, 180^\circ] \times [-80^\circ, 80^\circ]$, where the first dimension corresponds to the longitudes and the second to the latitudes. For the coherent set analysis, we select a Gaussian kernel $k(x, x') = \exp\left(-\frac{d(x, x')^2}{2\sigma^2}\right)$ with bandwidth $\sigma = 30$, where $d(x, x')$ is the distance between the points x and x' in kilometers computed with the aid of the haversine formula. The regularization parameter ε is set to 10^{-4} . The first two dominant eigenfunctions computed using kernel CCA are shown in Figure 4 (b) and (c) and a k -means clustering of the six dominant eigenfunctions in Figure 4 (d). CCA correctly detects the main gyres—the splitting of the South Atlantic Gyre and the Indian Ocean Gyre might be encoded in eigenfunctions associated with smaller eigenvalues—and the Antarctic Circumpolar Current. The clusters, however, depend strongly on the lag time τ . In order to illustrate the flow properties, typical trajectories are shown in Figure 4 (e). The trajectories belonging to different coherent sets remain mostly separated, although weak mixing can be seen, for instance, at the borders between the red and purple and red and green clusters.

3. Time-dependent energy potential

As a last example, we will analyze a molecular-dynamics inspired problem, namely diffusion in a time-dependent two-dimensional energy landscape, given by the stochastic differential equation

$$dX_t = -\nabla V(X_t, t) dt + \sqrt{2\beta^{-1}} dW_t,$$

with

$$V(x, t) = \cos\left(s \arctan(x_2, x_1) - \frac{\pi}{2}t\right)$$

ⁱ NOAA. What is a gyre? <https://oceanservice.noaa.gov/facts/gyre.html>

^j OceanParcels project: <http://oceanc parcels.org/>

^k GlobCurrent data repository: <http://www.globcurrent.org/>

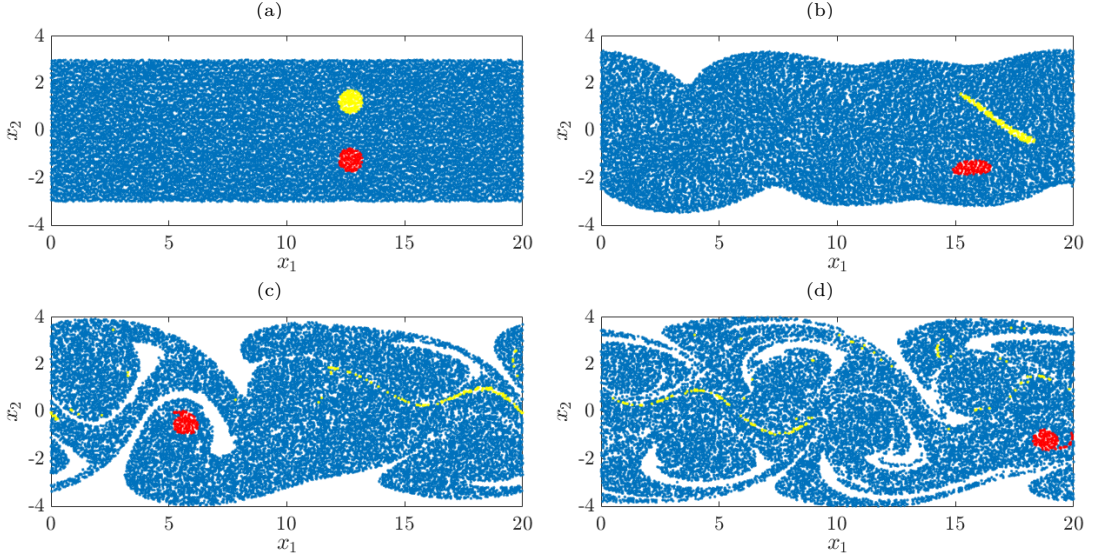


FIG. 2. Bickley jet at times (a) $t = 0$, (b) $t = 10$, (c) $t = 50$, and (d) $t = 100$ illustrating the difference between a non-coherent (yellow) and a coherent set (red). While the yellow set is dispersed after a short time, the shape of the red set remains nearly unchanged for a long time.

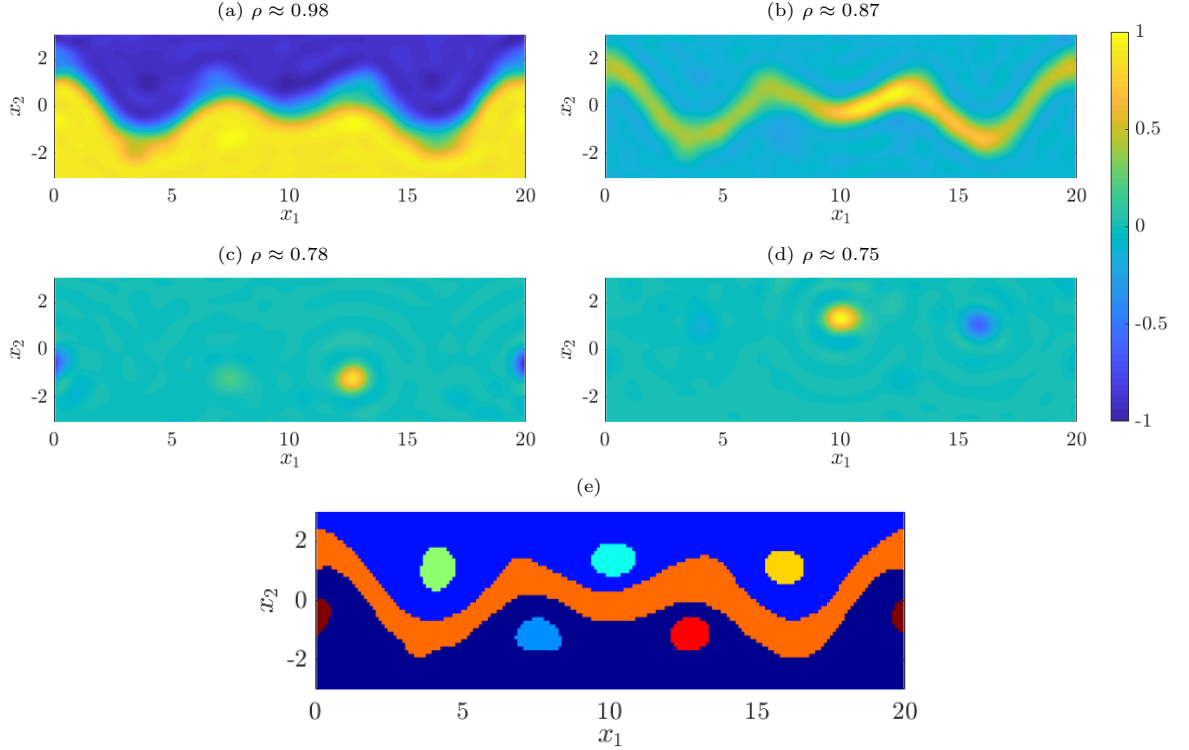


FIG. 3. (a) First, (b) second, (c) fourth, and (d) sixth eigenfunction associated with the Bickley jet for $\tau = 40$. (e) k -means clustering of the dominant eigenfunctions into nine coherent sets. Note that the red coherent set around $x = [12.5, -1.25]^\top$ corresponds to (but is not identical to) the red set in Figure 2, where we arbitrarily selected a perfectly circular shape.

$$+ 10 \left(\sqrt{x_1^2 + x_2^2} - \frac{3}{2} - \frac{1}{2} \sin(2\pi t) \right)^2.$$

The parameter β is the dimensionless inverse (absolute) temperature, W_t a standard Wiener process, and s spec-

ifies the number of wells. This is a generalization of a potential defined in Ref. 53, whose wells now move periodically towards and away from the center and which furthermore slowly rotates. We set $s = 5$. The resulting potential for $t = 0$ is shown in Figure 5 (a). Particles will

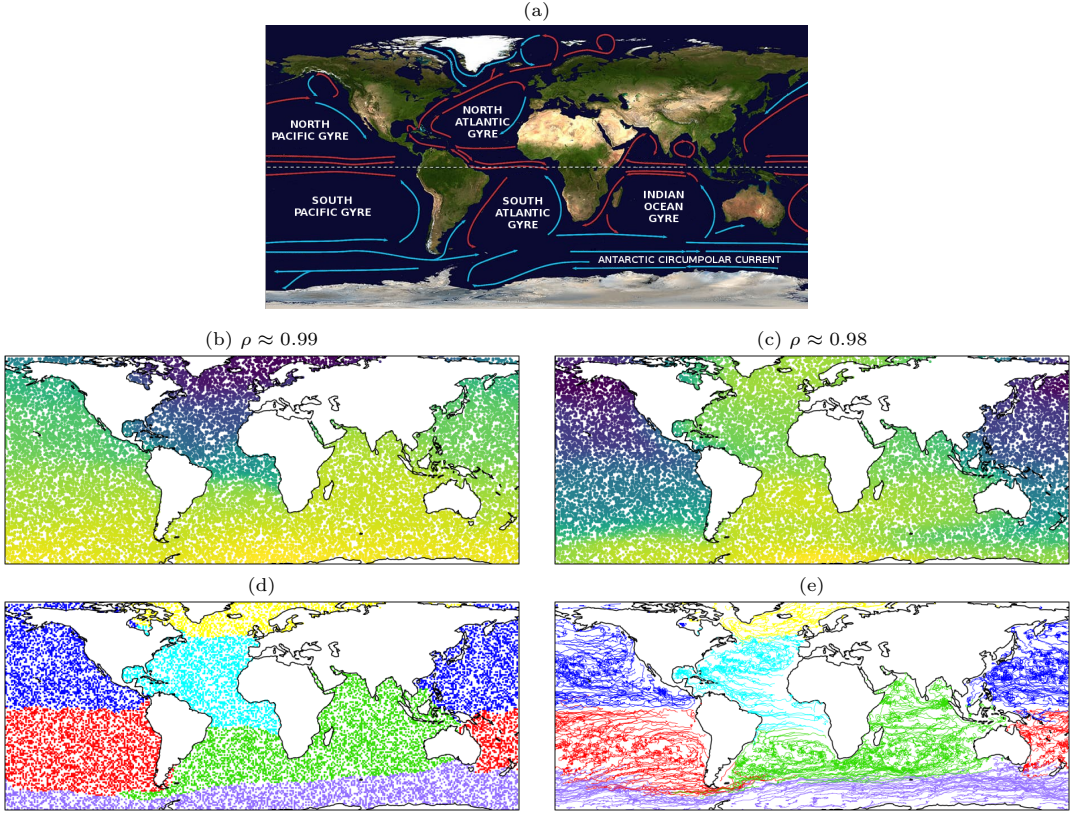


FIG. 4. (a) Illustration of the major ocean gyres (courtesy of NOAA). (b) First and (c) second eigenfunction. (d) k -means clustering of the first six eigenfunctions into six coherent sets. (e) Subset of the trajectories colored according to the coherent sets.

typically quickly equilibrate in radial direction towards the closest well and stay in this well, which moves over time. Particles trapped in one well will remain coherent for a relatively long time. The probability of escaping and moving to another one depends on the inverse temperature: The higher β , the less likely are transitions between wells.

We generate 1000 uniformly distributed test points in $\mathbb{X} = [-2.5, 2.5] \times [-2.5, 2.5]$ and integrate the system with the aid of the Euler–Maruyama method and the step size $h = 10^{-3}$ from $t = 0$ to $t = 10$. As before, we use only the start and end points of the trajectories and a Gaussian kernel (here, $\sigma = 1$ and $\varepsilon = 10^{-6}$) for the coherent set analysis.

Due to the centering of the Gram matrices, the eigenvalue $\lambda = 1$ vanishes and—depending on the parameter β —four eigenvalues close to one remain as illustrated in Figure 5 (b). Figure 5 (c) shows a clustering of the dominant four eigenfunctions for $\beta = 3$ based on PCCA+, resulting in the expected five coherent sets. The clustering at $t = 10$ (see Figure 5 (d)) illustrates that the computed sets indeed remain largely coherent.

Note that standard methods for the computation of metastable sets such as Ulam’s method, EDMD, or their variants are in general not suitable for non-equilibrium dynamics; see also Ref. 30 and Appendix A.

B. Coherent mode decomposition

In order to illustrate the coherent mode decomposition outlined in Algorithm III.7, we consider the classical von Kármán vortex street and generate data using a simple Python implementation.¹ It is important to note that here we take into account the full trajectory data $\{z_0, \dots, z_n\}$, where z_i is the state at time $t = 20i$, and define $X = [z_0, \dots, z_{n-1}]$ and $Y = [z_1, \dots, z_n]$, whereas we generated uniformly distributed data for the coherent set analysis in the previous subsection and furthermore used only the start and end points of the trajectories. We set $n = 100$ and $\varepsilon = 0.1$. Some snapshots of the system are shown in Figure 6 (a)–(d). Applying CMD results in the modes depicted in Figure 6 (e)–(g), where the color bar is the same as in Figure 3. As described above, we obtain two modes, denoted by ξ and η , for each eigenvalue ρ , where η can be interpreted as the time-lagged counterpart of ξ . There are three subdominant eigenvalues close to one, followed by a spectral gap. Removing the transient phase eliminates the third mode so that only the two highly similar modes remain.

¹ Palabos project: <http://wiki.palabos.org/numerics:codes>

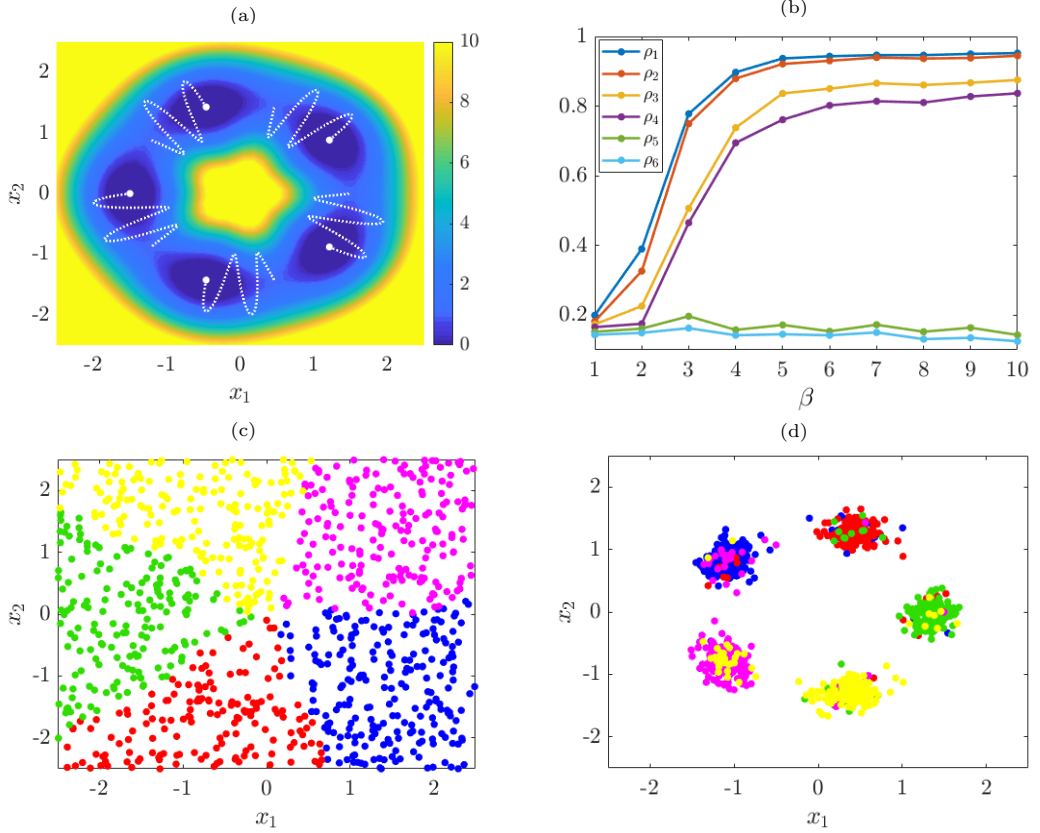


FIG. 5. (a) Time-dependent 5-well potential for $t = 0$. The dotted white lines indicate the periodic movement of the centers of the wells over time. (b) Dominant eigenvalues (averaged over multiple runs) as a functions of β . Coherence increases with increasing inverse temperature, i.e., the eigenvalues are closer to 1 for decreasing temperature. (c) Coherent set clustering for $\beta = 3$ at initial time $t = 0$. (d) Corresponding clustering at $t = 10$. The clusters moved but are still mostly coherent save for moderate mixing.

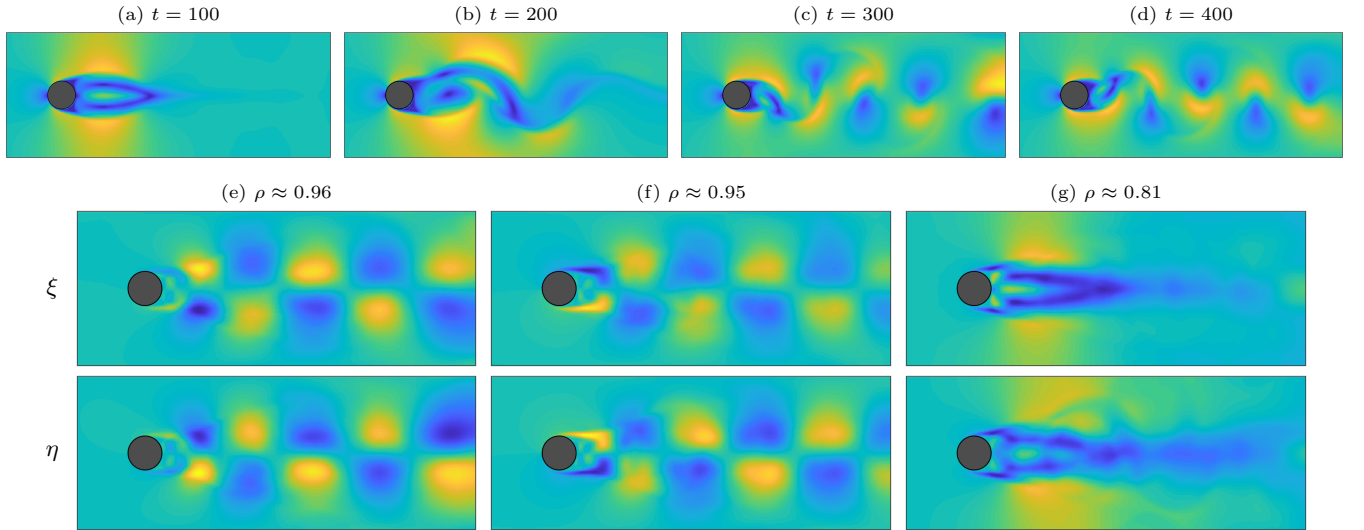


FIG. 6. (a)–(d) Two-dimensional flow in a channel past a cylinder. (e)–(g) Three subdominant coherent modes associated with the two-dimensional flow, where the top row contains the coherent modes ξ and the bottom row the corresponding modes η . The third mode is caused by the transient phase.

For this standard DMD benchmark problem, which we chose for illustration purposes, CMD and (regularized) DMD lead to almost identical modes. This might be—neglecting the transient phase—due to the periodicity of the system and the fact that we are applying the methods to sequential data. Nevertheless, CMD might have further applications pertaining to, for instance, non-sequential data, which we will investigate in future work.

V. CONCLUSION

We demonstrated that several kernel-based dimensionality reduction techniques can be interpreted as eigendecompositions of empirical estimates of certain RKHS operators. Moreover, we showed that applying CCA to Lagrangian data results in coherent sets and illustrated the efficiency of the methods using several examples ranging from fluid to molecular dynamics. This approach worked out of the box, although taking into account entire trajectories might improve the results even further, which would then necessitate dedicated kernels. In this work, we analyzed only low-dimensional benchmark problems. Nevertheless, the kernel-based algorithms can be easily applied to more complex problems and also non-vectorial domains such as graphs or strings.

As a byproduct of the coherent set analysis, we derived a method called CMD that is a hybrid of CCA and DMD (or TICA). This method can, for instance, be applied to high-dimensional fluid flow or video data. For specific problems, CMD and DMD—unsurprisingly, given the close proximity—result in highly similar modes. An interesting topic for future research would be to systematically analyze the relationships between these methods. Furthermore, as with the transfer operators and embedded transfer operators as well as their kernel-based estimates¹³, there are again several different combinations and variants of the proposed algorithms.

Another open problem is the influence of different regularization techniques on the numerical results. How does Tikhonov regularization compare to approaches based on pseudoinverses or other spectral filtering methods? And how do we choose the kernel and the regularization parameters in an optimal way, preferably without cross-validation? Additionally, future work includes analyzing the properties of the empirical estimate \hat{S} . Can we show convergence in the infinite-data limit? Which operators can be approximated by \hat{S} and can we derive error bounds for the resulting eigenvalues and eigenfunctions?

We expect the results in this paper to be a starting point for further theoretical research into how RKHS operators in the context of dynamical systems could be approximated and, furthermore, how they connect to statistical learning theory. Additionally, the methods proposed here might be combined with classical modifications of CCA in order to improve the numerical performance. The experiments here were performed using Matlab, and the methods have been partially reimplemented

in Python and are available at <https://github.com/sklus/d3s/>.

ACKNOWLEDGEMENTS

We would like to thank Péter Koltai for the Bickley jet implementation as well as helpful discussions related to coherent sets and Ingmar Schuster for pointing out similarities between CCA and kernel transfer operators. This research has been partially funded by Deutsche Forschungsgemeinschaft (DFG) through grant CRC 1114 *Scaling Cascades in Complex Systems*.

REFERENCES

- ¹B. Schölkopf, A. Smola, and K.-R. Müller. Nonlinear component analysis as a kernel eigenvalue problem. *Neural Computation*, 10(5):1299–1319, 1998.
- ²B. Schölkopf and A. J. Smola. *Learning with Kernels: Support Vector Machines, Regularization, Optimization and Beyond*. MIT press, Cambridge, USA, 2001.
- ³T. Melzer, M. Reiter, and H. Bischof. Nonlinear feature extraction using generalized canonical correlation analysis. In G. Dorffner, H. Bischof, and K. Hornik, editors, *Artificial Neural Networks — ICANN 2001*, pages 353–360, Berlin Heidelberg, 2001. Springer.
- ⁴F. R. Bach and M. I. Jordan. Kernel independent component analysis. *Journal of Machine Learning Research*, 3:1–48, 2003.
- ⁵S. Harmeling, A. Ziehe, M. Kawanabe, and K.-R. Müller. Kernel-based nonlinear blind source separation. *Neural Computation*, 15(5):1089–1124, 2003.
- ⁶C. R. Schwantes and V. S. Pande. Modeling molecular kinetics with tICA and the kernel trick. *Journal of Chemical Theory and Computation*, 11(2):600–608, 2015.
- ⁷J. Shawe-Taylor and N. Cristianini. *Kernel Methods for Pattern Analysis*. Cambridge University Press, 2004.
- ⁸I. Steinwart and A. Christmann. *Support Vector Machines*. Springer, New York, 1st edition, 2008.
- ⁹L. Song, J. Huang, A. Smola, and K. Fukumizu. Hilbert space embeddings of conditional distributions with applications to dynamical systems. In *Proceedings of the 26th Annual International Conference on Machine Learning*, pages 961–968, 2009.
- ¹⁰K. Muandet, K. Fukumizu, B. Sriperumbudur, and B. Schölkopf. Kernel mean embedding of distributions: A review and beyond. *Foundations and Trends in Machine Learning*, 10(1–2):1–141, 2017.
- ¹¹B. Koopman. Hamiltonian systems and transformation in Hilbert space. *Proceedings of the National Academy of Sciences*, 17(5):315, 1931.
- ¹²A. Lasota and M. C. Mackey. *Chaos, fractals, and noise: Stochastic aspects of dynamics*, volume 97 of

Applied Mathematical Sciences. Springer, 2nd edition, 1994.

¹³S. Klus, I. Schuster, and K. Muandet. Eigendecompositions of transfer operators in reproducing kernel Hilbert spaces. *ArXiv e-prints*, 2017.

¹⁴C. Schütte and M. Sarich. *Metastability and Markov State Models in Molecular Dynamics: Modeling, Analysis, Algorithmic Approaches*. Number 24 in Courant Lecture Notes. American Mathematical Society, 2013.

¹⁵J. N. Kutz, S. L. Brunton, B. W. Brunton, and J. L. Proctor. *Dynamic Mode Decomposition: Data-Driven Modeling of Complex Systems*. SIAM, 2016.

¹⁶Anton Bovier. Metastability: a potential theoretic approach. In *Proceedings of the International Congress of Mathematicians*, pages 499–518, 2006.

¹⁷G. Froyland and O. Junge. Robust FEM-based extraction of finite-time coherent sets using scattered, sparse, and incomplete trajectories. *SIAM Journal on Applied Dynamical Systems*, 17(2):1891–1924, 2018.

¹⁸G. Froyland and O. Junge. On fast computation of finite-time coherent sets using radial basis functions. *Chaos: An Interdisciplinary Journal of Nonlinear Science*, 25(8), 2015.

¹⁹M. O. Williams, I. I. Rypina, and C. W. Rowley. Identifying finite-time coherent sets from limited quantities of Lagrangian data. *Chaos: An Interdisciplinary Journal of Nonlinear Science*, 25(8), 2015.

²⁰A. Hadjighasem, D. Karrasch, H. Teramoto, and G. Haller. Spectral-clustering approach to Lagrangian vortex detection. *Physical Review E*, 93:063107, 2016.

²¹R. Banisch and P. Koltai. Understanding the geometry of transport: Diffusion maps for Lagrangian trajectory data unravel coherent sets. *Chaos: An Interdisciplinary Journal of Nonlinear Science*, 27(3):035804, 2017.

²²B. E. Husic, K. L. Schlueter-Kuck, and J. O. Dabiri. Simultaneous coherent structure coloring facilitates interpretable clustering of scientific data by amplifying dissimilarity. *PLoS ONE*, 14(3):e0212442, 2019.

²³M. R. Allshouse and T. Peacock. Lagrangian based methods for coherent structure detection. *Chaos: An Interdisciplinary Journal of Nonlinear Science*, 25(9):097617, 2015.

²⁴P. J. Schmid. Dynamic mode decomposition of numerical and experimental data. *Journal of Fluid Mechanics*, 656:5–28, 2010.

²⁵J. H. Tu, C. W. Rowley, D. M. Luchtenburg, S. L. Brunton, and J. N. Kutz. On dynamic mode decomposition: Theory and applications. *Journal of Computational Dynamics*, 1(2), 2014.

²⁶C. Baker. Mutual information for Gaussian processes. *SIAM Journal on Applied Mathematics*, 19(2):451–458, 1970.

²⁷C. Baker. Joint measures and cross-covariance operators. *Transactions of the American Mathematical Society*, 186:273–289, 1973.

²⁸J. R. Baxter and J. S. Rosenthal. Rates of convergence for everywhere-positive Markov chains. *Statistics & Probability Letters*, 22(4):333–338, 1995.

²⁹S. Klus, P. Koltai, and C. Schütte. On the numerical approximation of the Perron–Frobenius and Koopman operator. *Journal of Computational Dynamics*, 3(1):51–79, 2016.

³⁰P. Koltai, H. Wu, F. Noé, and C. Schütte. Optimal data-driven estimation of generalized Markov state models for non-equilibrium dynamics. *Computation*, 6(1), 2018.

³¹J. Mercer. Functions of positive and negative type and their connection with the theory of integral equations. *Philosophical Transactions of the Royal Society*, 209:415–446, 1909.

³²M. Reed and B. Simon. *Methods of Mathematical Physics I: Functional Analysis*. Academic Press Inc., 2 edition, 1980.

³³L. Rosasco, M. Belkin, and E. De Vito. On learning with integral operators. *Journal of Machine Learning Research*, 11:905–934, 2010.

³⁴C. W. Groetsch. *Inverse Problems in the Mathematical Sciences*. Vieweg, 1993.

³⁵H. Engl and C. W. Groetsch. *Inverse and Ill-Posed Problems*. Academic Press, 1996.

³⁶H. Engl, M. Hanke, and A. Neubauer. *Regularization of Inverse Problems*. Kluwer, 1996.

³⁷L. Song, K. Fukumizu, and A. Gretton. Kernel embeddings of conditional distributions: A unified kernel framework for nonparametric inference in graphical models. *IEEE Signal Processing Magazine*, 30(4):98–111, 2013.

³⁸K. Fukumizu, L. Song, and A. Gretton. Kernel Bayes’ rule: Bayesian inference with positive definite kernels. *Journal of Machine Learning Research*, 14:3753–3783, 2013.

³⁹K. Fukumizu. Nonparametric bayesian inference with kernel mean embedding. In G. Peters and T. Matsui, editors, *Modern Methodology and Applications in Spatial-Temporal Modeling*. 2017.

⁴⁰M. Mollenhauer, I. Schuster, S. Klus, and C. Schütte. Singular value decomposition of operators on reproducing kernel Hilbert spaces. *ArXiv e-prints*, 2018.

⁴¹John Shawe-Taylor, Christopher K. I. Williams, Nello Cristianini, and Jaz Kandola. On the eigenspectrum of the gram matrix and its relationship to the operator eigenspectrum. In *Algorithmic Learning Theory. ALT 2002. Lecture Notes in Computer Science*, vol 2533., pages 23–40, 11 2002.

⁴²S. Klus, A. Bittracher, I. Schuster, and C. Schütte. A kernel-based approach to molecular conformation analysis. *The Journal of Chemical Physics*, 149:244109, 2018.

⁴³M. Borga. Canonical correlation: a tutorial, 2001.

⁴⁴K. Fukumizu, F. Bach, and A. Gretton. Statistical consistency of kernel canonical correlation analysis. *Journal of Machine Learning Research*, 8:361–383, 2007.

⁴⁵M. O. Williams, I. G. Kevrekidis, and C. W. Rowley. A data-driven approximation of the Koopman operator: Extending dynamic mode decomposition. *Journal of Nonlinear Science*, 25(6):1307–1346, 2015.

⁴⁶M. O. Williams, C. W. Rowley, and I. G. Kevrekidis. A kernel-based method for data-driven Koopman spectral analysis. *Journal of Computational Dynamics*, 2(2):247–265, 2015.

⁴⁷F. Noé and F. Nüske. A variational approach to modeling slow processes in stochastic dynamical systems. *Multiscale Modeling & Simulation*, 11(2):635–655, 2013.

⁴⁸R. Penrose. A generalized inverse for matrices. *Mathematical Proceedings of the Cambridge Philosophical Society*, 51(3):406413, 1955.

⁴⁹S. Klus, F. Nüske, P. Koltai, H. Wu, I. Kevrekidis, C. Schütte, and F. Noé. Data-driven model reduction and transfer operator approximation. *Journal of Nonlinear Science*, 28:985–1010, 2018.

⁵⁰N. B. Erichson, L. Mathelin, S. L. Brunton, and N. J. Kutz. Randomized dynamic mode decomposition. *ArXiv e-prints*, 2017.

⁵¹I. I. Rypina, M. G. Brown, F. J. Beron-Vera, H. Koçak, M. J. Olascoaga, and I. A. Udovydchenkov. On the Lagrangian dynamics of atmospheric zonal jets and the permeability of the stratospheric polar vortex. *Journal of the Atmospheric Sciences*, 64(10):3595–3610, 2007.

⁵²M. Lange and E. van Sebille. Parcels v0.9: prototyping a Lagrangian ocean analysis framework for the petascale age. *Geoscientific Model Development*, 10(11):4175–4186, 2017.

⁵³A. Bittracher, P. Koltai, S. Klus, R. Banisch, M. Dellnitz, and C. Schütte. Transition manifolds of complex metastable systems: Theory and data-driven computation of effective dynamics. *Journal of Nonlinear Science*, 28(2):471–512, 2018.

⁵⁴S. Röblitz and M. Weber. Fuzzy spectral clustering by PCCA+: application to markov state models and data classification. *Advances in Data Analysis and Classification*, 7(2):147–179, 2013.

⁵⁵H. Wu and F. Noé. Variational approach for learning Markov processes from time series data. *ArXiv e-prints*, 2017.

⁵⁶A. Mardt, L. Pasquali, H. Wu, and F. Noé. VAMP-nets for deep learning of molecular kinetics. *Nature Communications*, 9(1):5, 2018.

⁵⁷F. Noé. Machine learning for molecular dynamics on long timescales. *ArXiv e-prints*, 2018.

⁵⁸F. Paul, H. Wu, M. Vossel, B. L. de Groot, and F. Noé. Identification of kinetic order parameters for non-equilibrium dynamics. *ArXiv e-prints*, 2018.

⁵⁹E. Kaiser, B. R. Noack, L. Cordier, A. Spohn, M. Segond, M. Abel, G. Daviller, J. Östh, S. Krajnović, and R. K. Niven. Cluster-based reduced-order modelling of a mixing layer. *Journal of Fluid Mechanics*, 754:365–414, 2014.

Appendix A: Relationships with VAMP

The use of CCA with nonlinear transformations of time-lagged data to calculate optimal low-rank approx-

imations of transfer operators was first described in Ref. 55 as the *variational approach for Markov processes* (VAMP). In VAMP, linear CCA is applied to the transformations, which are permitted to be of any form (e.g., obtained by a neural network⁵⁶). VAMP has thus been referred to as TCCA, i.e., time-lagged CCA^{30,55,57,58}. In the present work, on the other hand, we directly start with kernel CCA and show that it can be interpreted in terms of kernel transfer operators and, as a consequence thereof, detects coherent sets.

VAMP is designed to yield the optimal rank- k approximation of the transfer operator. VAMP is also equivalent to the generalized Markov state model (GMSM) approach described in Ref. 30 when determining an operator approximation with rank k . In both VAMP and GMSM, the *singular value decomposition* (SVD) is performed on $\widehat{\mathcal{C}}_{YY}^{-1/2} \widehat{\mathcal{C}}_{YX} \widehat{\mathcal{C}}_{XX}^{-1/2}$ to obtain the left and right singular vectors, where the inverse square roots are assumed to exist. The SVD here is equivalent to the eigendecomposition performed in the algorithm presented above (see Remark III.5). By trialing different basis sets, the sum of the highest k singular values raised to the r th power can be used to score the models, where the highest sum corresponds to the basis that yields the best approximation of the underlying dynamical processes in the resulting singular vectors⁵⁵. In the present work, if the feature spaces of the kernels corresponding to the data and time-lagged data are finite-dimensional and given explicitly, empirical estimates of the resulting eigenfunctions are equivalent to VAMP- r for $r = 1$. The advantage of the kernel-based variant is that it allows for implicitly infinite-dimensional feature spaces, which are determined by the kernel. When choosing a Gaussian kernel, for instance, the results depend only on the kernel bandwidth and a regularization parameter.

In Ref. 55, the dominant left and right singular vectors from VAMP are depicted for a nonreversible double-gyre system, but they are not discussed in the context of coherent structures or modes. In Ref. 30, GMSMs are generalized from the Markov state model (MSM) approximation to transfer operators developed for the analysis of reversible simulations of molecules with indicator function bases¹⁴. Due to reversibility, MSM matrix approximations to transfer operators are irreducible, so their eigenvalues are real due to the Perron–Frobenius theorem for irreducible matrices. In the context of reversible systems, the eigenvalues can be related to the timescales of dynamical processes. While similar methods have been used without reversibility—thus permitting imaginary eigenvalues (see, e.g., Ref. 59)—the GMSM method instead opts to use the SVD. The absence of the guarantee of real eigenvalues in the nonreversible case is viewed as a loss of interpretability, which is made up for by the connection of the singular values and vectors to the identification of coherent, instead of metastable, sets, such as in simulations along shifting potential energy surfaces.

Both the VAMP and GMSM approaches were designed to investigate Markovian dynamics, which is implicit in

the choice to use time-lagged pairs for analysis. Here, too, we restrict our analysis to time-lagged pairs, and thus can only capture dynamics explained by these two

views of the data. CCA and its kernel counterpart can be extended to more than two views of the data^{4,7}, but we leave this to future work.